TRENDS IN SCIENCES 2026; 23(7): 12607
https://doi.org/10.48048/tis.2026.12607 RESEARCH ARTICLE

Green Hydrothermal Synthesis of rGO/MnO_2 Nanocomposites from *Musa Paradisiaca Linn.* Peel Extract for High-Performance Supercapacitor Electrodes

Risma Aimatul Qudsiyah[1], Heydar Ruffa Taufiq[1], Priyono[1], Markus Diantoro[2], Agus Purwanto[3], Worawat Meevasana[4] and Agus Subagio[1,*]

[1]*Department of Physics, Faculty of Science and Mathematics, Diponegoro University, Semarang 50275, Indonesia*
[2]*Department of Physics, Faculty of Mathematics and Natural Science, Universitas Negeri Malang, Malang 65145, Indonesia*
[3]*Department of Chemical Engineering, Faculty of Engineering, Universitas Sebelas Maret, Central Java 57126, Indonesia*
[4]*Department of Physics, Faculty of Science, Suranaree University of Technology, Nakhon Ratchasima 30000, Thailand*

([*]Corresponding author's e-mail: agussubagio@lecturer.undip.ac.id)

Received: 10 November 2025, Revised: 19 December 2025, Accepted: 26 December 2025, Published: 5 March 2026

Abstract

The increasing global energy demand driven by population growth and urbanization has intensified the need for sustainable energy storage solutions. Supercapacitors are attractive candidates owing to their high power density, rapid charge–discharge capability, and long cycle life; however, the development of environmentally friendly electrode materials remains a challenge. In this work, banana peel extract was employed as a green reducing agent for the hydrothermal synthesis of reduced graphene oxide (rGO)/manganese dioxide (MnO_2) nanocomposites at 140, 160, and 180 °C. This green approach aims to minimize the use of hazardous chemicals while valorizing agricultural waste. Structural and morphological analyses confirmed the successful formation of the composite, with temperature-dependent phase transitions and distinct morphologies. Electrochemical measurements revealed that the rGO/MnO_2 electrode synthesized at 140 °C delivered the highest specific capacitance of 601.41 F g^{-1} at 0.5 A g^{-1}, outperforming those prepared at 160 °C (147.69 F g^{-1}) and 180 °C (549.09 F g^{-1}). These findings demonstrate that controlling the hydrothermal synthesis temperature significantly influences the composite's electrochemical properties. Therefore, banana peel-derived rGO/MnO_2 synthesized at 140 °C exhibits excellent capacitive performance, highlighting its potential as a sustainable electrode material for high-performance supercapacitors.

Keywords: Energy, Supercapacitors, rGO/MnO_2, Greensynthesis, Banana peel, Hydrothermal

Introduction

The increasing global energy demand, fueled by population growth, urbanization, and higher living standards, has made efficient and sustainable energy storage systems a critical priority Ma *et al*. [1]. The International Energy Agency (IEA) projects a 45% rise in energy demand by 2030, underscoring the urgency for innovative solutions that minimize environmental impact while meeting performance requirements Manohar *et al*. [2]. Supercapacitors have emerged as promising candidates due to their high power density, rapid charge-discharge capability, and long cycle life, making them suitable for applications in hybrid vehicles, portable electronics, and renewable energy integration Schoetz *et al*. [3]; Burak and Eldar [4]; Guntreddi *et al*. [5].

Supercapacitors store energy via two main mechanisms: Electric double-layer capacitance (EDLC), where energy is stored electrostatically at the electrode-electrolyte interface and pseudocapacitance (PC), which involves Faradaic redox reactions at the

electrode surface, such as those in MnO_2 Goljanian Tabrizi *et al*. [6]. EDLCs operate through a non-Faradaic reaction where ions are adsorbed onto the electrode surface to form an electric double layer. This process offers high energy density and long-term capacitance retention, albeit with the limitation of lower energy density Mo *et al*. [7]. For example, EDLC has demonstrated exceptional cycling stability, with 91.3% retention after 10,000 cycles at 5 A g^{-1} Reddygunta *et al*. [8]. In contrast, PC utilizes a Faradaic process that involves a redox reaction between the active material and electrolyte, such as MnO_2, which offers higher specific capacitance but often at the expense of reduced cycle stability Liu *et al*. [9].

Carbon-based materials, especially graphene and its derivatives, are widely used in supercapacitors due to their high electrical conductivity, large surface area, and chemical stability Lobato-Peralta *et al*. [10]. However, pristine graphene tends to aggregate, reducing its effective surface area and electrochemical performance Cossutta *et al*. [11]. Reduced graphene oxide (rGO) offers a practical alternative, combining graphene-like properties with easier synthesis via oxidation-exfoliation of graphite followed by reduction Miller *et al*. [12]. Despite its advantages, rGO still suffers from limited intrinsic capacitance due to restacking, necessitating composite formation with metal oxides like MnO_2, which provides high pseudocapacitance through Faradaic reactions but suffers from poor conductivity Rajalakshmi *et al*. [13]; Lamba *et al*. [14]; Li *et al*. [15]; Ramkumar *et al*. [16]. To address these limitations and promote sustainability, this study employs a one-step hydrothermal method using banana peel extract as a natural reducing agent, integrating biomass valorization with nanocomposite synthesis. The approach reduces hazardous chemical use and supports circular economy principles, while systematically investigating the impact of synthesis temperature on the structural and electrochemical properties of rGO/MnO_2 nanocomposites.

Banana peel (Musa paradisiaca Linn.), a widely available agricultural waste, possesses a fibrous and layered structure rich in polyphenols and reducing sugars, which are effective as natural reducing agents in nanomaterial synthesis Chaudhry *et al*. [17]. Research conducted by Buasuwan *et al*. [34] found that banana peel extracts effectively reduce graphene oxide, removing oxygen-containing functional groups and restoring sp^2 hybridized carbon networks Begum *et al*. [18] The fibrous morphology of Musa paradisiaca Linn. peel enhances the extraction efficiency of bioactive compounds and provides a favorable matrix for nanocomposite formation Buendía-Otero *et al*. [19]. This variety is selected due to its high content of polyphenols and reducing sugars, as well as its abundance in tropical regions, making it a sustainable and cost-effective raw material for green synthesis Pambudi *et al*. [20]. This approach not only reduces reliance on hazardous chemicals but also transforms agricultural waste into valuable energy storage materials, supporting circular economy principles Hikal *et al*. [21].

Existing methods for rGO/MnO_2 synthesis often rely on toxic reducing agents and multi-step procedures, limiting their environmental friendliness and scalability. This study introduces a one-step hydrothermal method using banana peel extract as a green reducing agent, directly integrating biomass valorization with nanocomposite synthesis. The selection of hydrothermal temperatures 140, 160, and 180 °C is based on previous studies demonstrating that this range significantly influences crystallinity, morphology, and interfacial properties, thereby directly impacting the electrochemical performance of supercapacitor electrodes. Research by Xia (2018) showed that temperatures between 140 and 180 °C are optimal for the effective reduction of graphene oxide, as thermal energy accelerates the removal of oxygen-containing functional groups and enhances the electrical conductivity of rGO Xia *et al*. [22]; Zhang *et al*. [23]. Further reported that this temperature range is ideal for the formation of crystalline MnO_2 with high surface area, while preventing thermal degradation of the rGO matrix Zhang *et al*. [23]; Salamon *et al*. [24] found that 160 °C yields a homogeneous distribution of MnO_2 nanoparticles on the rGO surface, maximizing synergistic effects between EDLC and pseudocapacitance Salamon *et al*. [24]. Moreover, selecting temperatures below 200 °C reduces energy consumption and maintains the effectiveness of banana peel polyphenols and flavonoids as natural reducing agents.

Existing methods for rGO/MnO_2 synthesis often rely on toxic reducing agents and multi-step procedures,

limiting their environmental friendliness and scalability. This study introduces a one-step hydrothermal method using banana peel extract as a green reducing agent, directly integrating biomass valorization with nanocomposite synthesis. The approach enables precise control over composite morphology and interface quality, with synthesis temperature as a key optimization parameter Khan *et al*. [25]. By systematically investigating the influence of temperature on crystal phase, morphology, and electrochemical performance Gan *et al*. [26]. This work bridges the gap between sustainable material sourcing and high-performance energy storage, providing a novel and environmentally responsible approach to supercapacitor electrode development. The characteristics of the rGO/MnO_2 composites were analyzed using X-ray diffraction (XRD) and scanning electron microscopy (SEM). At the same time, the electrochemical performance of the supercapacitor electrode materials was evaluated through cyclic voltammetry (CV), galvanostatic charge-discharge (GCD), and electrochemical impedance spectroscopy (EIS) measurements using an electrochemical workstation.

Materials and methods

Materials

KM_nO_4, graphite powder, HCl, H_2SO_4 (98%), H_2O_2 (39%), and $NaNO_3$ are analytical grades purchased from Merck, and banana peels were obtained from a synthesis.

Synthesis of graphene oxide

Graphene oxide was synthesized using the modified Hummers method, as described in previous research Anshori *et al*. [27]. Initially, 23.33 mL of H_2SO_4 solution was prepared in a beaker and stirred in an ice bath below 20 °C to control the exothermic reactions during the oxidation process, preventing material decomposition and the formation of unwanted by-products. Subsequently, 1 g of graphite powder and 0.5 g of $NaNO_3$ were added to the solution. A total of 5 g of $KMnO_4$ was gradually introduced while continuously stirring for 2 h on a hot plate. The temperature was then raised to 35 - 40 °C to accelerate the oxidation process and ensure a more homogeneous reaction, resulting in graphene oxide with a well-defined structure. The mixture was stirred for an additional 14 h to guarantee uniform distribution of reactants and facilitate complete oxidation, yielding high quality and stable graphene oxide. The color of the mixture changed to light brown and formed a paste-like consistency. Next, 41.6 mL of deionized (DI) water was added and stirred for 30 min to optimize the reaction. Oxidation was terminated by adding H_2O_2 solution, followed by dilution with 133 mL of DI water and 20 mL of 1 M HCl to remove excess sulfate ions. The resulting solid was filtered and dried in an oven at 80 °C. Finally, ultrasonication and centrifugation were performed to exfoliate the GO powder, producing well-dispersed graphene oxide nanosheets.

Preparation of banana peels extract

The banana peel used in this study was derived from *Musa paradisiaca Linn.* The peels were cleaned with tap water and thoroughly rinsed with deionized (DI) water to remove impurities. After cutting into small pieces (approximately 1 - 2 cm) to maximize the contact surface area during extraction, the pieces were dried in an air oven at 65 °C for 24 h to remove moisture without degrading bioactive compounds such as polyphenols and reducing sugars, which serve as natural reducing agents. Drying at this temperature was selected to prevent thermal decomposition of these compounds; higher temperatures or longer durations could compromise their reducing efficacy. The dried peels were then ground into a fine powder with a particle size of 100 - 200 μm and stored in a sealed container for subsequent use. This particle size was chosen to maximize the surface area for efficient extraction of reducing agents, directly influencing the release efficiency of polyphenols and reducing sugars, and supporting the formation of uniform and effective rGO/MnO_2 nanocomposites. Particles that are too large may reduce extraction efficiency, while those that are too small may cause agglomeration and handling difficulties. For extraction, 12 g of banana peel powder was mixed with 100 mL of DI water and stirred for 1 h at 70 °C. The mixture was centrifuged and filtered through Whatman filter paper. The resulting filtrate was preserved in a glass container at 4 °C for use in the synthesis of rGO/MnO_2 nanocomposites.

Synthesis of rGO/MnO_2 nanocomposite

The rGO/MnO_2 nanocomposite was synthesized using the in-situ hydrothermal method, as shown in **Figure 1**. Initially, 3.95 g $KMnO_4$, 4 mL 8 M H_2SO_4, and 75 mL deionized water were mixed using a magnetic stirrer at 35 °C for 30 min to ensure even distribution of reactants and facilitate optimal reduction between the natural reducing agent in the banana peel extract and the precursors (graphite oxide and MnO_2). A temperature of 35 °C was chosen to accelerate the reaction kinetics while minimizing the risk of thermal decomposition of bioactive compounds. Stirring was performed at 400 RPM to achieve homogeneity without causing excessive turbulence that could disrupt the nanocomposite structure. After that, 0.25 g of GO powder was added to the solution and stirred continuously for 30 min to ensure thorough mixing. The homogeneous mixture was then transferred to a Teflon-lined autoclave and hydrothermally treated at 140, 160, and 180 °C for 6 h. The resulting product was separated by centrifugation and washed repeatedly with deionized water until a neutral pH was achieved to remove residual contaminants. The precipitate was dried at 70 °C for 12 h, followed by grinding to obtain a fine rGO/MnO_2 nanocomposite powder with a particle size of 1 - 5 µm to maximize the active surface area, enhance electrolyte interaction and electrochemical performance, while avoiding excessive agglomeration that could reduce capacitance efficiency. The optimal surface area of the nanocomposite is crucial for supercapacitor applications, as it directly affects energy storage capacity and cycle stability.

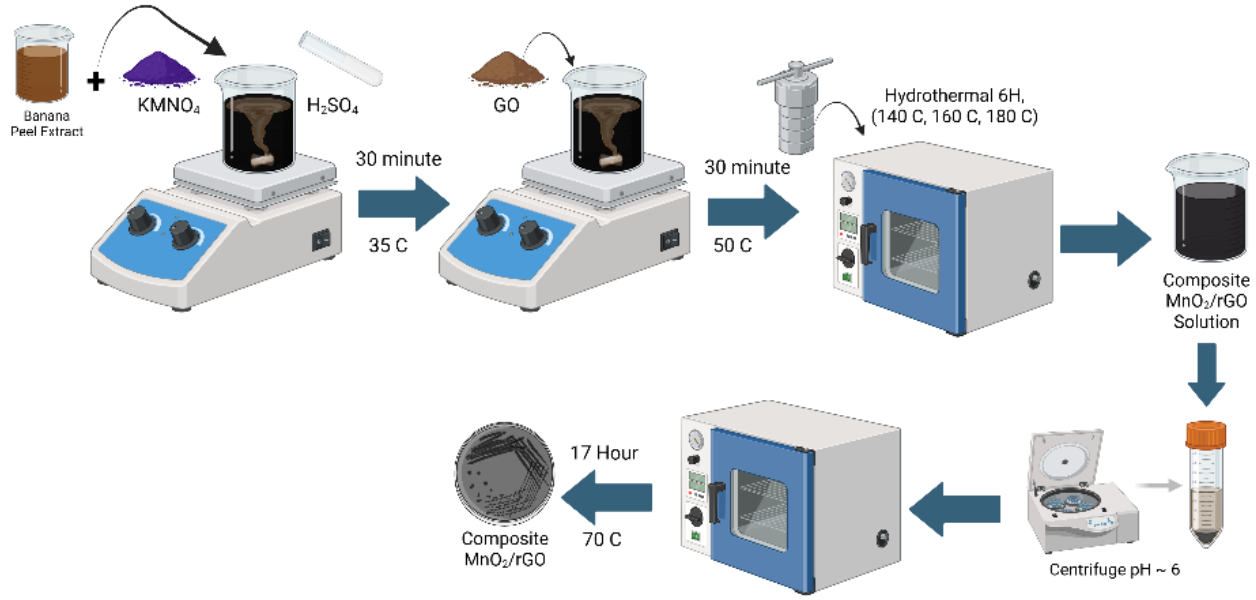

Figure 1 Synthesis of rGO/MnO_2 Nanocomposite.

Characterization

The structural and morphological characteristics of the synthesized rGO/MnO_2 composite were analyzed using several techniques. The crystalline structure of the composite was examined by X-ray diffraction (XRD, Rigaku D/MAX-2500/PC, Cu Kα radiation, λ = 1.54 Å) operated at 40 kV, to determine the phase composition and degree of crystallinity of the carbon-based materials. The surface morphology and microstructural features of the composite were observed using scanning electron microscopy (SEM, JEOL JSM-6510LA), which provided detailed information on the dispersion of MWCNTs within the activated carbon matrix and the surface texture of the electrode.

Electrodes modification

The electrochemical sensing element (electrochemical sensor) consists of 3 electrodes: GCE as the working electrode (WE), Ag/AgCl reference electrode (RE), and Pt wire as the counter electrode. To prepare the nanomaterial suspension, 14 mg of rGO/MnO_2 140, 160, and 180 °C were added to 2 mL of

distilled water and ethanol (material to solvent ratio 7:1). The mixture was then homogenized in an ultrasonic bath. The drop-casting technique was used for electrode modification. The sensor was modified after dripping 5 µL of nanomaterial suspension over WE and adding 5 µL of Nafion solution, left to dry at 27 °C (room temperature) until ensuring loading of the prepared material Madagalam *et al*. [29]; Ristiana *et al*. [28].

Electrochemical Characterization

The electrochemical properties of rGO/MnO_2 nanocomposites were studied by galvanostatic charge-discharge (GCD), electrochemical impedance spectroscopy (EIS), cyclic voltammetry (CV), and retention measurements using a PalmSens4 potentiostat and PSTrace BETA 5.10 application. The tests were conducted in 1M H_2SO_4 solution. A three-electrode setup was used for the measurements Chebrolu *et al*. [30]; Ristiana *et al*. [28]. CV testing was carried out to determine the supercapacitor mechanism by looking at the cyclic shape of the material in the potential range of 0 - 1 V at various scan rates of 5, 10, 25, 50, 75, and 100 mVs^{-1}. GCD testing was performed to calculate specific capacitance (Cs), energy density (E), and power density (P) at various current densities of 0.5, 1.0, 2.5, 5.0, 7.5, and 10.0 A g^{-1}. EIS testing was conducted in the frequency range of 0.1 Hz to 10 kHz.

In GCD testing, the results of charging and discharging analysis are used to calculate specific capacitance (Cs), energy density (E), and power density (P). Retention testing is carried out to determine the ability of supercapacitors to maintain capacitance and performance during repeated charge and discharge cycles Seman *et al*. [31] so that supercapacitors can be used effectively in long-term applications without experiencing a significant decrease in work Hsiao *et al*. [32].

Results and discussion

This study presents a green, one-step hydrothermal synthesis of reduced graphene oxide/manganese dioxide (rGO/MnO_2) nanocomposites using banana peel extract as a natural reducing agent. The process simultaneously reduces graphene oxide (GO) and facilitates the nucleation of MnO_2 nanostructures through a redox reaction between $KMnO_4$ and the carbon framework of GO in an 8M HCl acidic medium. The acidic environment plays a crucial role in controlling the morphology and crystallinity of MnO_2 Dong *et al*. [33]. At the same time, bioactive compounds in the banana peel extract (e.g., flavonoids, ascorbic acid) contribute to the efficient reduction of GO to rGO Buasuwan *et al*. [34]. Under acidic conditions, the nucleation reaction follows the Eq. (1):

$$4KMnO_4+3C+4HCl \rightarrow 4MnO_2+3CO_2+4KCl+2H_2O \quad (1)$$

The MnO_2 nuclei formed then undergo growth through a hydrolysis mechanism:

$$4KMnO_4+2H_2O \rightarrow 4MnO_2+4KOH+3O_2 \quad (2)$$

The nucleation and growth of the MnO2 structure are sensitive to pH, indicating the importance of controlling acidic conditions in determining the final morphology of MnO2 A'Yuni *et al.* [35]. XRD performed the structural characterization of the samples. **Figure 2** shows the XRD patterns of GO and rGO/MnO_2 nanocomposites synthesized at different hydrothermal temperatures.

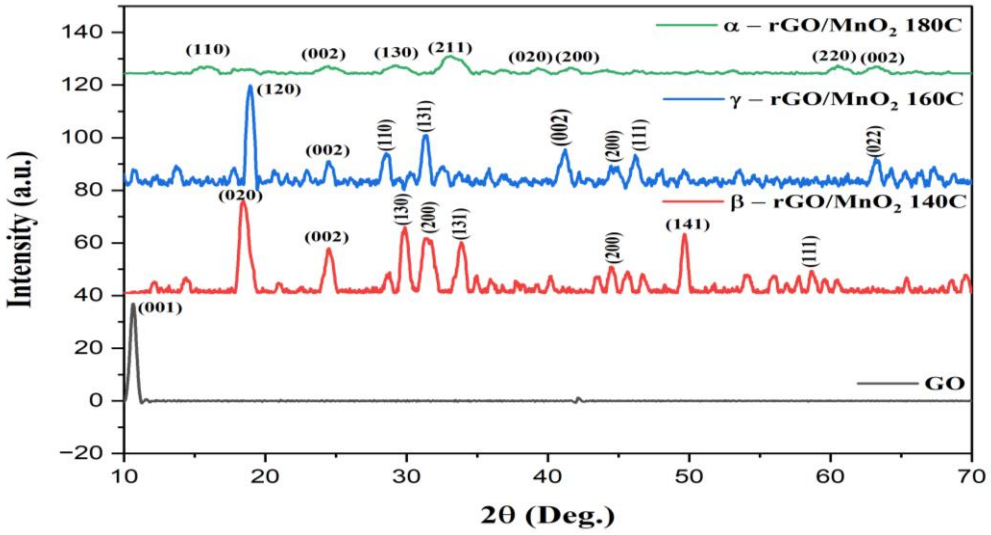

Figure 2 XRD patterns of GO, β-rGO/MnO_2 140 °C, γ – rGO/MnO_2 160 °C, α- rGO/MnO_2 180 °C.

The XRD pattern of GO shows a characteristic peak at 10.65°, corresponding to the (001) plane, confirming successful oxidation with an interlayer spacing of approximately 0.892 nm, typical of oxygen-functionalized graphene sheets Hamade *et al*. [36]; Ristiana *et al*. [28]. After reduction and composite formation with MnO_2, sharp and well-defined diffraction peaks appear, indicating the formation of crystalline MnO_2. At 140 °C, the composite exhibits peaks at 2θ values of 18.46°, 29.88°, 31.3°, 33.86°, 44.5°, 49.66°, and 58.7°, attributed to the (020), (130), (200), (131), (141), and (111) planes, respectively, corresponding to the β-MnO_2 (pyrolusite) phase (tetragonal, space group P 42/m n m) Yugambica *et al*. [37]. The relatively low peak intensity indicates incomplete crystallization, consistent with previous studies reporting limited crystallinity at lower hydrothermal temperatures.

At 160 °C, the XRD pattern shows improved crystallinity with sharper and more intense peaks at 2θ values of 18.94°, 28.58°, 31.42°, 44.48°, 48.08°, and 63.18°, corresponding to the (120), (110), (131), (002), (111), and (002) planes, respectively, confirming the formation of a stable γ-MnO_2 phase (tetragonal, JCPDS 0440141) Yugambica *et al*. [37]. At 180 °C, the composite exhibits the highest crystallinity with very sharp and intense peaks at 2θ values of 14.66°, 27.12°, 32.58°, 42.65°, 60.52°, and 63.26°, corresponding to the (110), (130), (211), (020), (220), and (002) planes, respectively, confirming the formation of the α-MnO_2 phase (tetragonal, space group I4/m). The disappearance of the GO peak in all composites confirms successful reduction to rGO, while the emergence of broad peaks at 23° - 25° (002) and 40° - 42° (200) indicates successful reduction to rGO, with the broad nature of these peaks suggesting the formation of disordered few-layer rGO with reduced interlayer spacing and partial restoration of the π-conjugated system Rusi and Majid [38].

The reduction in XRD peaks at 180 °C compared to 140 and 160 °C is due to increased aggregation and larger MnO_2 crystal size, resulting in decreased intensity and broader diffraction peaks. This is in line with research conducted by Rani *et al*. [39] showing that at a hydrothermal temperature of 180 °C, MnO_2 particle agglomeration and partial degradation of the rGO structure occur, causing broadening of the XRD diffraction peak and a decrease in intensity, indicating damage to the crystallinity of the nanocomposite Rani *et al*. [39]. In addition, high temperatures can cause partial degradation of the rGO structure, which further reduces its contribution to the diffraction peak. These structural changes explain the lower electrochemical performance of the nanocomposite at 180 °C compared to lower temperatures Ingole *et al*. [41]; Mohamad [40].

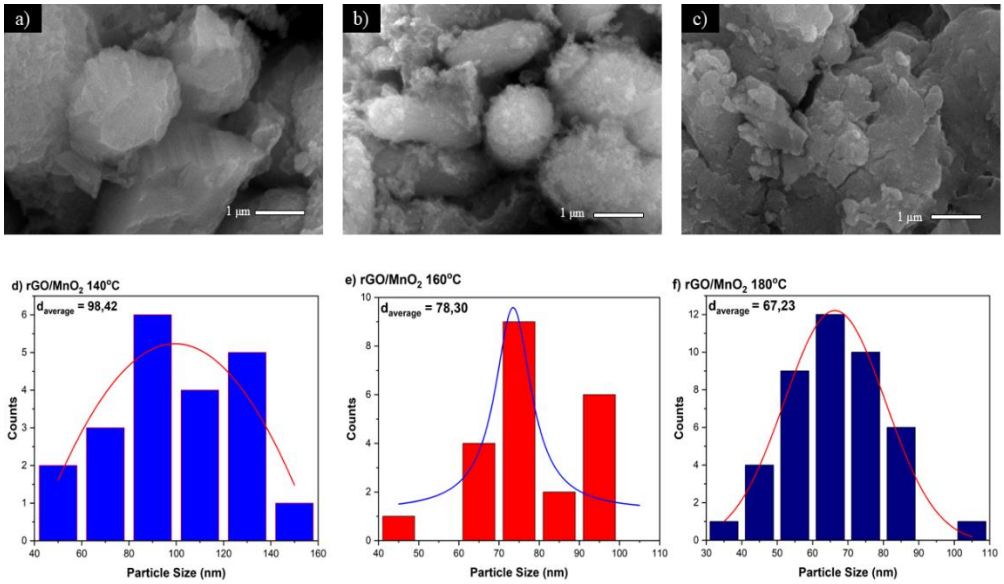

Figure 3 SEM morphology of rGO/MNO$_2$ at (a) 140 °C, (b) 160 °C, and (c) 180 °C; particle size distribution of rGO/MnO$_2$, (d) 140 °C, (e) 160 °C, and (f) 180 °C.

Morphological analysis using SEM (Scanning Electron Microscopy) on the rGO/MnO$_2$ composite shows significant structural changes as the hydrothermal temperature increases. At a hydrothermal temperature of 140 °C as shown in **Figure 3(a)**, MnO$_2$ particles can be seen with a relatively large round to oval shape with a rather smooth and compact surface. The particle size in this condition tends to be non-uniform with uneven distribution over the rGO surface. This is consistent with the research of Wang *et al*. [42] who reported that low hydrothermal temperatures produce MnO$_2$ particles with sizes varying between 320 nm distributed on rGO sheets Wang *et al*. [42].

Increasing the hydrothermal temperature to 160 °C, as seen in **Figure 3(b)**, shows a noticeable morphological transformation, where the MnO$_2$ particles become smaller and better dispersed on the rGO surface. The structure formed shows the characteristics of particles with a more irregular shape and aggregated with each other to form a spongy structure. This phenomenon is by the findings of Rondiya *et al*. [43], who observed that MnO$_2$ nanorods have a width ranging from 5,070 nm with an average length of 1 µm under optimal synthesis conditions Rondiya *et al*. [43]. The improvement in particle dispersion at this temperature indicates a better interaction between MnO$_2$ and the rGO matrix.

At the highest hydrothermal temperature of 180 °C seen in **Figure 3(c)**, the morphology of the composite shows the most homogeneous structure with very small MnO$_2$ particles evenly distributed across the rGO surface. The structures formed exhibit nanoflower-like characteristics with minimal aggregation, suggesting that high temperatures facilitate the formation of more organized crystal structures. Research by Lozano-Steinmetz *et al*. [44] confirmed that rGO/MnO$_2$ composites with optimized morphology show improved thermal properties due to the 2D structure of rGO, which has a thermal conductivity two orders of magnitude higher than the metal oxide Lozano-Steinmetz *et al*. [44]. This change in morphology is also in line with XRD results that show an increase in crystallinity at the same temperature, indicating a close relationship between crystal structure and surface morphology in determining the properties of composite materials.

The particle size distribution processed using Gaussian fitting shows that each rGO/MnO$_2$ sample shows a different particle size distribution at synthesis temperatures of 140, 160, and 180 °C. The Gaussian distribution on the particle size histogram provides a statistical description of the average particle diameter ($d_{average}$) and the level of uniformity (polydispersity) of the particles formed. At 140 °C, the average particle size was recorded at 98.42 nm, with a relatively wide and not very symmetrical distribution, indicating a considerable

variation in particle size. At 160 °C, the average particle size decreased to 78.30 nm, and the distribution appeared narrower, indicating more uniform particles. While at 180 °C, the average particle size decreased again to 67.23 nm with a better and symmetrical Gaussian distribution, indicating a higher level of uniformity.

The use of the Gaussian approach in SEM analysis is essential to understand the characteristics of the particle size distribution, as a near-Gaussian distribution signifies a controlled synthesis process and produces particles of uniform size Lin *et al*. [46]; Peng *et al*. [45]. A narrow, near-Gaussian particle size distribution can improve the functional properties of the material, such as high specific surface area and good interphase contact, thus greatly supporting the performance of rGO/MnO_2-based supercapacitor electrodes (Lin *et al*. [46]; Shahid *et al*. [47]. In addition, the Gaussian distribution also facilitates statistical evaluation and reduction of measurement uncertainty from SEM results, so that the results obtained are more representative of the actual particle population Chiang [48]; Peng *et al*. [45]. Thus, the analysis of Gaussian-based particle size distribution from SEM images provides important information related to the optimization of the synthesis process and the potential performance of the material as a supercapacitor electrode.

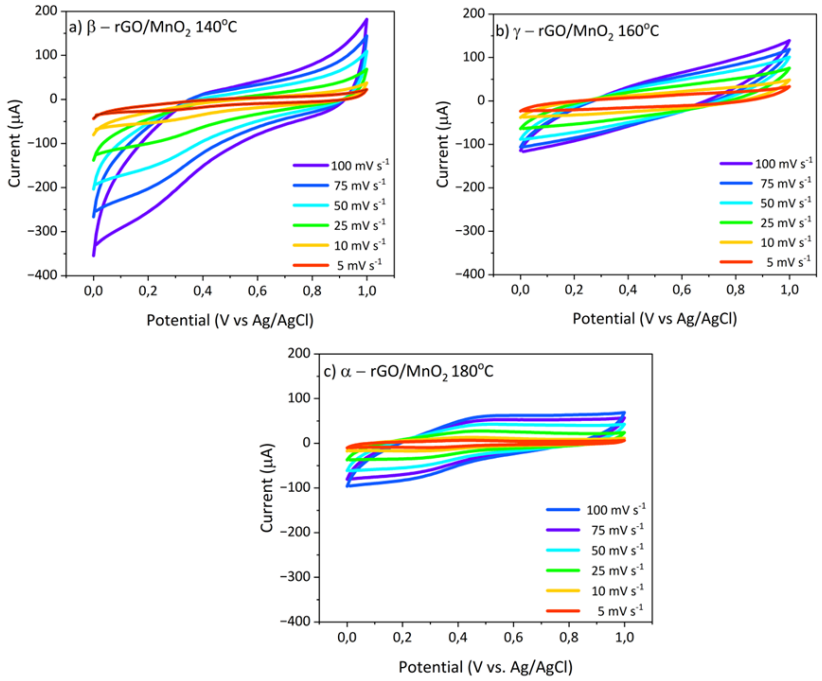

Figure 4 Cyclic Voltammetry Scan Rate Curves of 100 - 5 mV s^{-1} rGO/MnO_2 temperature (a) 140 °C, (b) 160 °C, and (c) 180 °C.

Cyclic voltammetry (CV) analysis of reduced graphene oxide/MnO_2 (rGO/MnO_2) composites reveals exceptional electrochemical properties, making them promising candidates for supercapacitor electrodes. The CV curves exhibit distinct redox peaks at approximately 0.2 V and –0.1 V (vs. reference electrode), corresponding to the reversible Mn^{2+}/Mn^{3+} redox transition. Notably, the rGO/MnO_2 composite demonstrates a significantly enhanced current response compared to pristine MnO_2, indicative of improved charge transfer kinetics and more efficient utilization of electroactive Mn species (Rusi and Majid 2015)[38]. At lower scan rates, the composite exhibits pronounced pseudocapacitive behavior, characterized by well-defined Faradaic reactions. However, as the scan rate increases, the CV profiles progressively adopt a more rectangular shape, suggesting a shift toward capacitive-dominated charge storage mechanisms Kalaiarasi *et al*. [49].

The results of cyclic voltammetry (CV) testing on rGO/MnO_2 electrodes at various hydrothermal temperatures show typical electrochemical

characteristics for supercapacitor applications. At 140 °C, as shown in **Figure 4(a)**, the CV curve of β-rGO/MnO_2 shows a near rectangular shape at various scan rates, indicating good capacitive behavior and efficient charge storage capability Yugambica *et al*. [37]; Saravanan *et al*. [50]. The 140 °C calcination temperature maintains the ideal rGO/MnO_2 heterostructure, where MnO_2 particles are evenly distributed on the rGO surface without excessive agglomeration Çepni and Öznülüer [51]. At this temperature, the material achieves an optimal balance between structural integrity and electronic interaction, facilitating efficient electron transfer and reversible Faradaic processes, despite the moderate crystallinity of MnO_2. This results in superior supercapacitor performance, characterized by high current responseandstable charge storage.

In contrast, the γ–rGO/MnO_2 composite synthesized at 160 °C, as shown in **Figure 4(b)**, demonstrates improved MnO_2 crystallinity and more uniform particle distribution on rGO sheets, yet exhibits a reduced CV area compared to the 140 °C sample. This suggests that higher temperatures ma compromise interfacial interactions between rGO and MnO_2, leading to lower current density while retaining capacitive behavior and electrochemical stability.

The increase in MnO_2 crystallinity and specific surface area at 180 °C is consistent with the results of research conducted by Shinde *et al*. [52], which shows that at this temperature, even though crystallinity increases, excessive agglomeration can limit electroactive sites and ion access, which affects charge storage capacity Shinde *et al*. [52]. This trend is supported by previous studies. In this study, the absence of such additives and the dominance of the α-MnO_2 phase at 180 °C contribute to the observed trend, aligning with the majority of the literature on hydrothermal synthesis of MnO_2-based composites Ran *et al*. [53].

These findings underscore the critical role of hydrothermal temperature in tailoring the structural, interfacial, and electrochemical properties of rGO/MnO_2 composites. 140 °C emerges as the optimal condition, maximizing capacitive performance by balancing conductivity, redox activity, and nanostructural synergy.

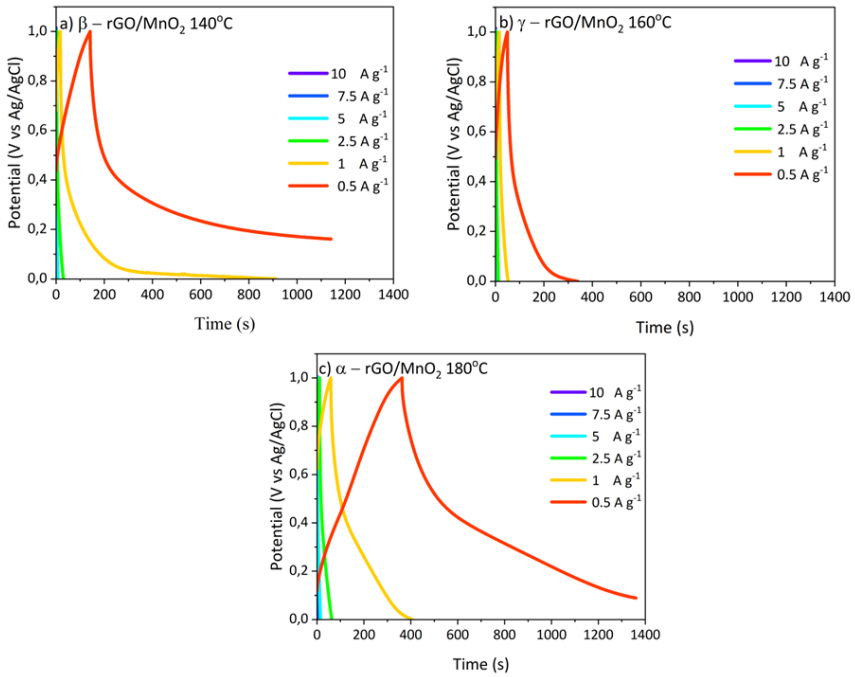

Figure 5 GCD analysis graph (a) β - rGO/MnO_2 140 °C, (b) γ - rGO/MnO_2 160C, (c) α - rGO/MnO_2 180 °C, and (d) GCD graph at potential range of 0.5 A g^{-1}.

Galvanostatic charge–discharge (GCD) is a widely used method to evaluate the electrochemical performance of energy storage electrodes. The GCD profiles of rGO/MnO_2 nanocomposites synthesized at

140, 160, and 180 °C (**Figure 5**) exhibit distinct voltage–time characteristics at various current densities (0.5, 1, 2.5, 5, 7.5, and 10 A g^{-1}). The profile at 0.5 A g^{-1} is notably different, showing a longer discharge time and higher specific capacitance compared to higher current densities. This behavior occurs because, at lower current densities, ion diffusion and redox reactions proceed more completely, allowing maximum access to the active sites within the nanocomposite. In contrast, at higher current densities, ion diffusion is limited, and only the outer surface of the material participates in charge storage, resulting in shorter discharge times and reduced capacitance Apriwandi *et al*. [54].

This trend is consistent with previous studies, where the specific capacitance of rGO/MnO_2 composites typically decreases with increasing current density due to restricted ion diffusion and higher internal resistance at elevated currents Ristiana *et al*. [28]. The GCD curves for all samples remain relatively symmetric, indicating good reversibility and high coulombic efficiency. The nearly linear shape of the curves suggests a dominant electric double-layer capacitance (EDLC) mechanism, with minor curvature indicating a contribution from pseudocapacitance due to MnO_2 [49]. The clear difference observed at 0.5 A g^{-1} highlights the excellent electrochemical kinetics of the nanocomposite at low current densities, which is characteristic of high-performance supercapacitor electrodes.

In particular, higher current densities result in steeper slopes in the GCD curves. By carefully studying these GCD characteristics, the specific capacitance of the supercapacitor can be determined using Eq. (3) Peçenek *et al*. [55]:

$$C_s = \frac{I \times \Delta t}{m \times \Delta V} \quad (3)$$

where m is the mass of the active electrode material, ΔV is the potential window in which the GCD measurement is recorded, I is the current applied during the GCD measurement, and Δt is the discharge time of the supercapacitor.

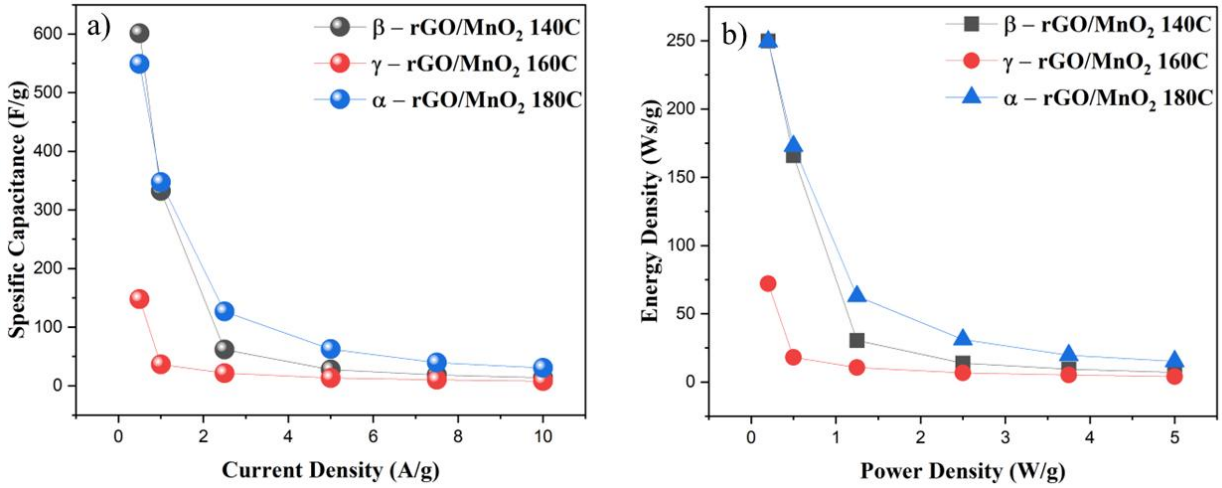

Figure 6 (a) Specific capacitance vs. current density and (b) Ragone plot of β-rGO/MnO_2 composites at 140 °C, γ-rGO/MnO_2 at 160 °C, and α-rGO/MnO_2 at 180 °C.

In **Figure 6(a)** the β-rGO/MnO_2 140 °C electrode produces the highest specific capacitance of 601.41 F g^{-1} at a current density of 0.5 A g^{-1}. At γ-rGO/MnO_2 160 °C, the specific capacitance value is much lower than that of β-rGO/MnO_2 140 °C at all current densities, with the highest value of only 147.69 F g^{-1}. However, at 180 °C, α-rGO/MnO_2 has a higher value than γ-rGO/ MnO_2 at 160 °C, which is 549.09 F g^{-1}. β-rGO/MnO_2 at 140 °C has a higher specific capacitance value compared to materials hydrothermally synthesized at higher temperatures. This phenomenon can be attributed to the stability of the structure and optimal pore distribution at lower hydrothermal temperatures Taer *et al*. [56].

GCD tests at several power densities were performed to plot the Ragone plots presented in **Figure 6(b)**. At a power density of 0.2 W g^{-1}, rGO/MnO_2 140

°C shows a high energy density of 249.89 W s g^{-1}, while rGO/MnO_2 160 °C shows a lower energy density of 72.08 W s g^{-1}. However, the rGO/MNO_2 at 180 °C shows a better value than the 160 °C, namely an energy density of 249.56 W s g^{-1}. The relatively small IR drop in all material variations indicates low internal resistance, which indicates good ionic and electronic conductivity Kalaiarasi *et al*. [49]; Taer *et al*. [56]. This is very important for practical applications because the low internal resistance will improve the energy efficiency and power density of the supercapacitor device. The stable GCD profile over a wide range of current densities also indicates good electrochemical stability, which is a critical parameter for long-term applications Wang *et al*. [42]; Zhang *et al*. [58].

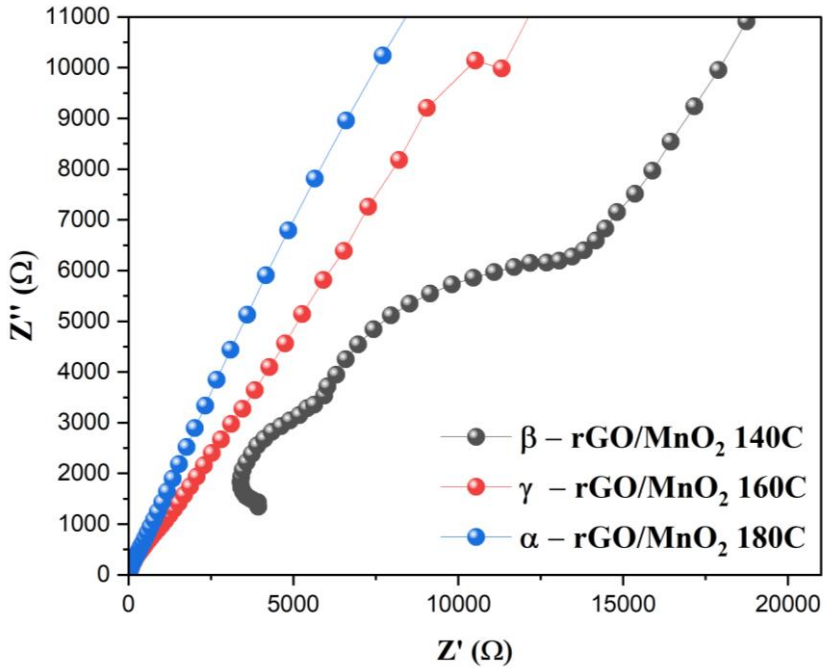

Figure 7 Nyquist plot of β-rGO/MnO_2 composite material at 140 °C, γ-rGO/MnO_2 at 160 °C, and α-rGO/MnO_2 at 180 °C.

The results of the Electrochemical Impedance Spectroscopy (EIS) test are shown in **Figure 7**. β-rGO / MnO_2 140 °C has a clearer semicircle and almost forms a semicircle on the Nyquist plot compared to samples at 160 and 180 °C. The semicircle on the Nyquist plot describes the electron transfer resistance (Rct) at the interface of the electrode and electrolyte. The smaller the diameter of the semicircle, the lower the Rct value, indicating a more efficient charge transfer process at the electrode Kalaiarasi *et al*. [49]. The β-rGO/MnO_2 at 140 °C exhibits prominent semicircle characteristics, indicating a balance between charge transfer resistance and double-layer capacitance. This indicates that the electrode at 140 °C has an optimal structure and interface contact, so that the redox process and charge storage are more effective. This phenomenon is in line with reports in international journals, where rGO/MnO_2 nanocomposites can improve supercapacitor performance through a combination of electrical double capacitance from rGO and pseudocapacitive capacitance from MnO_2 Rusi and Majid [38]; Kalaiarasi *et al*. [49].

The green synthesis approach utilizing banana peel waste as a reducing agent not only aligns with circular economy principles but also offers significant cost advantages compared to conventional methods that rely on hazardous chemicals. Banana peel is an abundant and low-cost agricultural waste, widely available in tropical regions, which reduces raw material expenses and minimizes environmental impact. The extraction and synthesis processes require only basic laboratory equipment, further lowering operational costs. The resulting rGO/MnO_2 nanocomposites demonstrate competitive electrochemical performance,

as shown in **Table 1**, highlighting the efficacy of temperature-controlled phase engineering in enhancing energy storage metrics. This cost-effective and environmentally friendly approach underscores the potential of banana peel-based supercapacitor systems as a sustainable alternative for future energy storage technologies, supporting both economic and ecological goals.

Table 1 The specific capacitance values of rGO/MnO_2 electrodes are reported in references.

Synthesis method	Spesific capacitance ($F\ g^{-1}$)	Current density ($A\ g^{-1}$)	References
rGO/MnO_2 Hydrothermal (nanorod)	398	1	Salamon *et al*. [24]
rGO/MnO_2 Electrodeposition + EPD	432	0.5	Kang *et al*. [59]
CNT/rGO/MnO_2	404	1	Lu *et al*. [60]
rGO/MnO_2 greensynthesis hydrothermal method	601, 41	0.5	This work

Conclusions

This study successfully demonstrates a green, one-step hydrothermal synthesis of reduced graphene oxide/manganese dioxide (rGO/MnO_2) nanocomposites using banana peel extract as a natural reducing agent. The use of banana peel waste not only aligns with sustainable and environmentally friendly principles but also offers an effective approach to reducing hazardous chemical usage in nanomaterial synthesis. Structural and morphological analyses confirmed the formation of distinct MnO_2 phases and morphologies at different hydrothermal temperatures, with XRD and SEM results indicating that the synthesis temperature critically affects the composite's crystalline phase and nanostructure.

Electrochemical characterization revealed that the rGO/MnO_2 nanocomposite synthesized at 140 °C exhibits the highest specific capacitance (601.41 F g^{-1} at 0.5 A g^{-1}), outperforming those synthesized at 160 and 180 °C. This superior performance is attributed to the optimal phase and morphology achieved at this temperature, which enhances electrochemical activity and charge storage capability. The results highlight the potential of banana peel-derived rGO/MnO_2 nanocomposites as high-performance, eco-friendly electrode materials for next-generation supercapacitors.

Overall, this research provides a significant contribution to the development of sustainable energy storage materials by integrating green chemistry with advanced nanotechnology. The findings demonstrate that biomass waste valorization through green synthesis routes can yield high-quality functional materials, supporting the advancement of environmentally responsible energy solutions. However, further studies are needed to optimize the scalability of the synthesis process, enhance long-term cycling stability under real-world conditions, and refine electrode architecture for higher energy density. Additionally, the impact of varying banana peel sources and extraction methods on the properties of nanocomposites should be systematically investigated to ensure reproducibility and consistency. Addressing these limitations will be crucial for improving the performance and practical applicability of banana peel-based supercapacitor systems.

Acknowledgements

The authors wish to thank Universitas Diponegoro, Indonesia for providing research funding through the Riset Kolaborasi Indonesia (RKI)-2022 (contract no. 434-14/UN7.D2/PT/IV/2022)

Declaration of Generative AI in Scientific Writing

The authors acknowledge the use of Perplexity AI for literature assistance and Grammarly for language editing and grammar correction. These tools were used solely to improve clarity and language quality. The authors are fully responsible for the content and conclusions of the manuscript.

CRediT Author Statement

Risma Aimatul Qudsiyah: Conceptualization, Methodology, Data Curation, Investigation, Formal Analysis, Validation, Visualization, and Writing – original draft. **Heydar Ruffa Taufiq:** Methodology,

Project administration, Resources, Supervision, and Validation. **Priyono:** Data curation, Formal analysis, Investigation, Validation, and Visualization. **Markus Diantoro:** Investigation, Validation, and Visualization. **Agus Purwanto**: Investigation, Validation, and Visualization. **Worawat Meevasana:** Investigation, Validation, and Visualization. **Agus Subagio:** Conceptualization, Methodology, Supervision, Validation, and Funding acquisition.

References

[1] S Ma, S Li, Q Luo, Z Yu and Y Wang. Revisiting the relationships between energy consumption, economic development and urban size: A global perspective using remote sensing data. *Heliyon* 2024; **10(5)**, e27318.

[2] A Manohar, V Vijayakanth, SVP Vattikuti and KH Kim. Synthesis and characterization of Mg2+ substituted MnFe2O4 nanoparticles for supercapacitor applications. *Ceramics International* 2022; **48(20)**, 30695-30703.

[3] T Schoetz, LW Gordon, S Ivanov, A Bund, D Mandler and RJ Messinger. Disentangling faradaic, pseudocapacitive, and capacitive charge storage: A tutorial for the characterization of batteries, supercapacitors, and hybrid systems. *Electrochimica Acta* 2022; **412**, 140072.

[4] A Burak and D Eldar. Sustainable power solutions: Renewable energy & storage advancements. *Journal of Science & Technology* 2024; **4(6)**, 13-34.

[5] V Guntreddi, V Manoj, MR Reddy, N Kumar Yegireddy, A Swathi and R Raghutu. Storage solutions for sustainable future: Integrating batteries, supercapacitors, and thermal storage. *E3S Web of Conferences* 2024; **547**, 03016.

[6] AG Tabrizi, N Arsalani, A Mohammadi, H Namazi, LS Ghadimi and I Ahadzadeh. Facile synthesis of a MnFe2O4/rGO nanocomposite for an ultra-stable symmetric supercapacitor. *New Journal of Chemistry* 2017; **41 (12)**, 4974-4984.

[7] X Mo, G Xu, X Kang, H Yin, X Cui, Y Zhao, J Zhang, J Tang and F Wang. A facile microwave hydrothermal synthesis of ZnFe2O4/rGO nanocomposites for supercapacitor electrodes. *Nanomaterials* 2023; **13(6)**, 1034.

[8] KKR Reddygunta, R Beresford, L Šiller, L Berlouis and A Ivaturi. Activated carbon utilization from corn derivatives for High-energy-density flexible supercapacitors. *Energy and Fuels* 2023; **37(23)**, 19248-19265.

[9] J Liu, J Wang, C Xu, H Jiang, C Li and L Zhang. Advanced energy storage devices: Basic principles, analytical methods, and rational materials design. *Advanced Science* 2018; **5(1)**, 1700322.

[10] DR Lobato-Peralta, PU Okoye and C Alegre. A review on carbon materials for electrochemical energy storage applications: State of the art, implementation, and synergy with metallic compounds for supercapacitor and battery electrodes. *Journal of Power Sources* 2024; **617**, 235140.

[11] M Cossutta, V Vretenar, TA Centeno, P Kotrusz, J McKechnie and SJ Pickering. A comparative life cycle assessment of graphene and activated carbon in a supercapacitor application. *Journal of Cleaner Production* 2020; **242**, 118468.

[12] EE Miller, Y Hua and FH Tezel. Materials for energy storage: Review of electrode materials and methods of increasing capacitance for supercapacitors. *Journal of Energy Storage* 2018; **20**, 30-40.

[13] R Rajalakshmi, KP Remya, C Viswanathan and N Ponpandian. Enhanced electrochemical activities of morphologically tuned $MnFe_2O_4$ nanoneedles and nanoparticles integrated on reduced graphene oxide for highly efficient supercapacitor electrodes. *Nanoscale Advances* 2021; **3(10)**, 2887-2901.

[14] P Lamba, P Singh, P Singh, A Kumar, P Singh, Bharti, Y Kumar and M Gupta. Simple and rapid eco-friendly synthesis of NiO/rGO nanocomposites using guava leaf extract and their physicochemical characterization. *Materials Today: Proceedings* 2022; **68(7)**, 2705-2714.

[15] Q Li, M Liu, F Huang, X Zuo, X Wei, S Li and H Zhang. Co_9S_8@MnO_2 core–shell defective heterostructure for high-voltage flexible supercapacitor and Zn-ion hybrid supercapacitor. *Chemical Engineering Journal* 2022; **437**, 135494.

[16] R Ramkumar, S Suganthi, A Milton, J Park, J Shim, TH Oh and WK Kim. MnO/Mn_2O_3 aerogels as effective materials for supercapacitor applications. *Energies* 2024; **17(10)**, 2258.

[17] F Chaudhry, ML Ahmad, Z Hayat, MMAN Ranjha, KChaudhry, N Elboughdiri, M Asmari and J Uddin. Extraction and evaluation of the antimicrobial activity of polyphenols from banana peels employing different extraction techniques. *Separations* 2022; **9(7)**, 165.

[18] SS Begum, I Suyambulingam, P Senthamaraikannan, SH Suhailuddin, K Aprajith and R Kumar. Biofiber from Musa paradisiaca L. peduncle biomass waste: Extraction and characterization for polymer composites suitability study. *Journal of Natural Fibers* 2024; **21(1)**, 2433039.

[19] MJ Buendía-Otero, DJ Jiménez-Corzo, ZICD Ávila and JB Restrepo. Chromatographic analysis of phytochemicals in the peel of Musa paradisiaca to synthesize silver nanoparticles. *Revista Facultad de Ingeniería* 2022; **103**, 130-137.

[20] NA Pambudi. Optimization of hydrothermal processing for banana peel waste: Enhancing solid fuel characteristics as a renewable energy source. *Results in Engineering* 2025; **26**, 104831.

[21] WM Hikal, HAHSA Ahl, A Bratovcic, KG Tkachenko, J Sharifi-Rad, M Kačániová, M Elhourri and M Atanassova. Banana peels: A waste treasure for human being. *Evidence-Based Complementary and Alternative Medicine* 2022; **2022**, 7616452.

[22] Y Xia, J Wang, C Chen, D Huo, Y Wen, W Wang, M Sun, C Xu, A Xie, F Wu and Z Feng. Controlled hydrothermal temperature provides tunable permittivity and improved electromagnetic absorption performance of reduced graphene oxide. *RSC Advances* 2018; **8(58)**, 33065-33071.

[23] X Zhang, T Zhang, H Chen and Y Cao. A review of online electrochemical diagnostic methods of on-board proton exchange membrane fuel cells. *Applied Energy* 2021; **286**, 116481.

[24] J Salamon, A Simi, HJ Prabu, AF Sahayaraj, AJS Kennedy and J Beny. Synthesis and characterization of rGO-anchored MnO_2 nanorods and their application in supercapacitors as electrode material. *Journal of Electronic Materials* 2025; **54**, 510-522.

[25] M Khan, M Salman, A Ullah, N Ullah, A Syed and AH Bahkali. Effect of hydrothermal reaction temperature on MoO_3 nanostructure properties for enhanced electrochemical performance as an electrode material in supercapacitors. *Ceramics International* 2024; **50(19)**, 34943-34955.

[26] YX Gan, AH Jayatissa, Z Yu, X Chen and M Li. Hydrothermal synthesis of nanomaterials. *Journal of Nanomaterials* 2020; **2020**, 8917013.

[27] I Anshori, KA Kepakisan, LN Rizalputri, RR Althof, AE Nugroho, RA Siburian and M Handayani. Facile synthesis of graphene oxide/Fe3O4 nanocomposite for electrochemical sensing on determination of dopamine. *Nanocomposites* 2022; **8**, 155-166.

[28] DD Ristiana, M Handayani, MA Anggoro, BW Widagdo, E Angelina and H Sutanto. Reduced graphene oxide/nano-silica (rGO/n-SiO_2) nanocomposite for electrode materials of supercapacitor with high cycling stability. *South African Journal of Chemical Engineering* 2024; **48**, 130-137.

[29] M Madagalam, M Rosito, N Blangetti, M Etzi, E Padovano and B Bonelli. Unveiling the effect of Bi in $ZnFe_2O_4$ nanoparticles in electrochemical sensors. *Applied Surface Science* 2024; **640**, 160870.

[30] VT Chebrolu, D Jang, GM Rani, C Lim, K Yong and WB Kim. Overview of emerging catalytic materials for electrochemical green ammonia synthesis and process. *Carbon Energy* 2023; **5**, e361.

[31] MA Azam, RNAR Seman, MA Mohamed and MH Ani. Effect of polytetrafluoroethylene binder content on gravimetric capacitance and life cycle stability of graphene supercapacitor. *International Journal of Automotive and Mechanical Engineering* 2022; **19(3)**, 9964-9970.

[32] C Hsiao, C Lee and N Tai. High retention supercapacitors using carbon nanomaterials/iron oxide/nickel–iron layered double hydroxides as electrodes. *Journal of Energy Storage* 2022; **46**, 103805.

[33] X Dong, X Wang, J Wang, H Song, X Li and L Wang, MB Chan-Park, CM Li and P Chen.

Synthesis of a MnO_2–graphene foam hybrid with controlled MnO_2 particle shape and its use as a supercapacitor electrode. *Carbon* 2012; **50(13)**, 4865-4870.

[34] L Buasuwan, V Niyomnaitham and A Tandaechanurat. Reduced graphene oxide using environmentally friendly banana extracts. *MRS Advances* 2019; **4**, 2143-2151.

[35] DQ A'Yuni, I Alkian, FK Sya'Diyah, Kadarisman, A Darari and V Gunawan. Structural characterization of hydrothermally synthesized MnO_2 nanorods. *Journal of Physics: Conference Series* 2017; **909(1)**, 012004.

[36] F Hamade, E Radich and VA Davis. Microstructure and electrochemical properties of high performance graphene/manganese oxide hybrid electrodes. *RSC Advances* 2021; **11**, 34302-34312.

[37] S Yugambica, MAC Dhanemozhi and S Iswariya. Synthesis and characterization of MnO_2/rGO nanocomposite for supercapacitors. *International Research Journal of Engineering and Technology* 2017; **4(4)**, 1738-1743.

[38] Rusi and SR Majid. Green synthesis of in situ electrodeposited rGO/MnO_2 nanocomposite for high energy density supercapacitors. *Scientific Reports* 2015; **5**, 16195.

[39] P Rani, R Dahiya, M Bulla, R Devi, K Jeet and A Jatrana. Hydrothermal-assisted green synthesis of reduced graphene oxide nanosheets using lemon (Citrus limon) peel extract. *Materials Today: Proceedings* 2023; **80**, 2475-2481.

[40] AA Mohamad. Cyclic voltammetry of hybrid supercapacitors: A characterization review. *Inorganic Chemistry Communications* 2025; **172**, 113677.

[41] RS Ingole, SL Kadam, R Kamat, JG Ok and SB Kulkarni. Synthesis and electrochemical characterizations of rGO-decorated MnO_2 nanorods/carbon cloth-based wearable symmetric supercapacitors. *Surfaces and Interfaces* 2024; **52**, 104976.

[42] X Wang, Z Jiang, X Huang, L Sun and Y Wang. Surface topography prediction and reliability analysis of ball end milling. *Measurement* 2025; **242**, 115770.

[43] SR Rondiya, I Karbhal, CD Jadhav, MP Nasane, TE Davies and MV Shelke. Uncovering the origin of enhanced field emission properties of rGO–MnO_2 heterostructures: A synergistic experimental and computational investigation. *RSC Advances* 2020; **10(43)**, 25988-25998.

[44] F Lozano-Steinmetz, MP Ramírez-Navarro, L Vivas, DA Vasco, DP Singh and C Zambra-Sazo. Thermal and rheological characterization of aqueous nanofluids based on reduced graphene oxide with manganese dioxide nanocomposites. *Nanomaterials* 2022; **12(17)**, 3042.

[45] H Peng, C Luo, L He and H Tang. Embedded particle size measurement method of metal mineral polished section using Gaussian mixture model based on expectation maximization algorithm. *Minerals* 2024; **14(4)**, 358.

[46] F Lin, Y Liu, X Li and C Bai. Numerical and experimental investigation of particle size distribution produced by an electrical discharge process. *Materials* 2021; **14(2)**, 287.

[47] M Shahid, TR Katugampalage, M Khalid, W Ahmed, C Kaewsaneha and P Sreearunothai. Microwave-assisted synthesis of Mn_3O_4 nanograins intercalated into reduced graphene oxide layers as cathode material for alternative clean power generation energy device. *Scientific Reports* 2022; **12**, 23622.

[48] C Chiang. Discussion on measurement uncertainty evaluation: Applied to SEM with liquid cell for particle size measurement of liquid nanoparticles. *Journal of Nanotechnology Research* 2024; **6(2)**, 27-34.

[49] S Kalaiarasi, S Shyamala, M Kavitha, C Vedhi and RR Muthuchudarkodi. Electrochemical performance of reduced graphene oxide-based MnO_2 nanocomposite for supercapacitor. *Nanosystems: Physics, Chemistry, Mathematics* 2022; **13(3)**, 320-330.

[50] A Saravanan, P Arunachalam, GR Reddy and V Vijayan. Development of MnO_2/rGO composite electrodes for enhanced electrochemical supercapacitor performance. *Journal of New Materials for Electrochemical Systems* 2024; **27(3)**, 208-214.

[51] E Çepni and T Öznülüer Özer. Electrochemical deposition of indium(III) hydroxide

nanostructures for novel battery-like capacitive materials. *Journal of Energy Storage* 2022; **45**, 103678.

[52] DP Shinde, YA Pathak, AT Mane, DH Bobade, GM Hingangavkar and SL Tamboli. Unravelling the role of synthesis temperature in δ-MnO_2 nanosphere formation for high-performance supercapacitors. *ChemistrySelect* 2025; **10(16)**, e202500904.

[53] J Ran, Y Liu, T Yang, H Feng, H Zhan and H Shi. MnO_2@MoS_2/rGO hollow structure as high-performance supercapacitor electrode materials. *Journal of Energy Storage* 2023; **64**, 107216.

[54] A Apriwandi, E Taer and R Farma. Analysis of cyclic voltammetry and galvanostatic charge–discharge electrode supercapacitor based on activated carbon from Kepok banana leaf (Musa balbisiana). *Journal of Aceh Physics Society* 2021; **10(4)**, 94-101.

[55] H Peçenek, S Yetiman, FK Dokan, MS Onses, E Yılmaz and E Sahmetlioglu. Effects of carbon nanomaterials and MXene addition on the performance of nitrogen-doped MnO_2-based supercapacitors. *Ceramics International* 2022; **48(5)**, 7253-7260.

[56] E Taer, H Eva Wahyuni, A Apriwandi and T Rika. Electrochemical performance of aqueous electrolytes in porous carbon derived from cassava peel electrode materials for sustainable symmetrical supercapacitors. *Journal of Applied Materials and Technology* 2023; **4(1)**, 1-10.

[57] Y Wang, W Lai, N Wang, Z Jiang, X Wang and P Zou. Reduced graphene oxide/mixed-valence manganese oxide composite electrode for tailorable and surface-mountable supercapacitors with high capacitance and super-long life. *Energy & Environmental Science* 2017; **10(4)**, 941-949.

[58] Y Zhang, X Li, Z Li and F Yang. Evaluation of electrochemical performance of supercapacitors from equivalent circuits through cyclic voltammetry and galvanostatic charge–discharge. *Journal of Energy Storage* 2024; **86**, 111122.

[59] DN Kang, J Li, YH Xu and WX Huang. Synthesis of MnO_2 nanoparticle-decorated graphene-based porous composite electrodes for high-performance supercapacitors. *International Journal of Electrochemical Science* 2020; **15(7)**, 6091-6108.

[60] L Lu, S Xu, J An and S Yan. Electrochemical performance of CNTs/RGO/MnO_2 composite material for supercapacitor. *Nanomaterials and Nanotechnology* 2016. https://doi.org/10.1177/1847980416663687